HHS Public Access

Author manuscript

Nat Catal. Author manuscript; available in PMC 2019 August 27.

Published in final edited form as:

Nat Catal. 2019 February ; 2: 164–173. doi:10.1038/s41929-018-0217-z.

Catalytic hydrogen atom transfer from hydrosilanes to vinylarenes for hydrosilylation and polymerization

Parham Asgari[1], **Yuanda Hua**[1], **Apparao Bokka**[1], **Chanachon Thiamsiri**[2], **Watcharapon Prasitwatcharakorn**[2], **Ashif Karedath**[1], **Xin Chen**[3], **Sinjinee Sardar**[1], **Kyungsuk Yum**[4], **Gyu Leem**[5], **Brad S. Pierce**[1], **Kwangho Nam**[1,6], **Jiali Gao**[7], **Junha Jeon**[1,*]

[1]Department of Chemistry and Biochemistry, The University of Texas at Arlington, Arlington, Texas 76019, USA [2]Department of Chemistry, Mahidol University, Bangkok, 10400, Thailand [3]Theoretical Chemistry Institute, Jilin University, Changchun, Jilin Province 130023, People's Republic of China [4]Department of Materials Science and Engineering, University of Texas at Arlington, Arlington, Texas 76019, USA [5]Department of Chemistry, State University of New York–College of Environmental Science and Forestry, Syracuse, NY 13210, USA [6]Department of Chemistry, Umeå University, Umeå SE-901 87, Sweden [7]Department of Chemistry, University of Minnesota, Minneapolis, MN 55455, USA

Abstract

Because of the importance of hydrogen atom transfer (HAT) in biology and chemistry, there is increased interest in new strategies to perform HAT in a sustainable manner. Here, we describe a sustainable, net redox-neutral HAT process involving hydrosilanes and alkali metal Lewis base catalysts — eliminating the use of transition metal catalysts — and report an associated mechanism concerning Lewis base-catalysed, complexation-induced HAT (LBCI-HAT). The catalytic LBCI-HAT is capable of accessing both branch-specific hydrosilylation and polymerization of vinylarenes in a highly selective fashion, depending on the Lewis base catalyst used. In this process, earth abundant, alkali metal Lewis base catalyst plays a dual role. It first serves as a HAT initiator and subsequently functions as a silyl radical stabilizing group, which is critical to highly selective cross-radical coupling. EPR study identified a potassiated paramagnetic

*jjeon@uta.edu

Author contributions

P.A., Y.H. and J.J. conceived the project, designed the experiments and wrote the manuscript. P.A. and Y.H. performed NMR and GC studies. Y.H., P.A., A.B., C.T. and W.P. further developed the reaction and expanded the scope. Y.H. performed the radical clock and the corresponding control experiments. B.S.P., P.A. and S.S. performed the EPR studies. J.G., K.N. and X.C. conducted the computational studies. G.L., P.A., K.Y., and A.K. carried out synthesis and analysis of polymers. All authors discussed the results and commented on the manuscript. P.A. and Y.H. contributed equally to this work.

Additional information

Supplementary information and chemical compound information are available in the online version of the paper. Reprints and permissions information is available online at www.nature.com/reprints. Publisher's note: Springer Nature remains neutral with regard to jurisdictional claims in published maps and institutional affiliations. Correspondence and requests for materials should be addressed to J.J.

Competing financial interests

The authors declare no competing financial interests.

species and multistate density function theory revealed a high HAT character, yet multiconfigurational nature in the transition state of the reaction.

Graphical Abstract

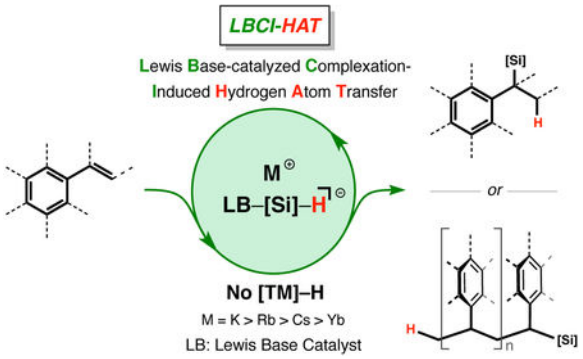

Hydrogen atom transfer (HAT) — a concerted migration of a proton and electron from a donor to an acceptor molecule in a single kinetic step — is ubiquitous and one of the most fundamental chemical processes in chemistry and biology.[1, 2] Examples include regio and stereoselective processes catalysed by transition metal catalysts [1, 3, 4] (Figure 1a) and in the active sites of metalloenzymes (e.g., cytochrome P450s and non-heme Fe and Cu oxidases).[5, 6] In chemical synthesis, HAT is closely related to free radical chemistry, often called hydrogen atom abstraction, and typically involves in the termination step of radical reactions between group 14 metal(oid) hydrides and carbon-centred radicals.[4] Despite substantial advances in this field, the wide and sustainable application of current thermal radical chemistry are hindered by the need for a stoichiometric amount of toxic reducing agents (e.g., organotin hydrides), excess solvent, and operational inconvenience.

First-row transition metal hydrides[7, 8] bearing relatively weak metal-hydride (M–H, M: Fe, Mn, Co) bonds (ca. 40–70 kcal/mol) allow a facile generation of carbon-centred radicals from olefins by HAT.[9, 10] Although such a process has been recently shown to be remarkably useful for catalytic olefin hydrofunctionalization (Figure 1a),[1, 4, 11–14] a more sustainable approach toward elimination of the use of transition metals for the HAT would be development of catalytic methods harnessing low-cost, environmentally benign catalysts. In this view, we considered organosilicon hydrides as an alternative hydrogen source for HAT. Our hypothesis is based on Corriu's pioneering works concerning a wide range of chemical reactivity of pentacoordinate silicates (e.g., $M[HSiL_4]$, M = Li, Na, K, NR_4).[15] In the studies, the Lewis base-activation strategy of hydrosilanes was capable of both a single electron transfer (SET) and two-electron reduction chemistry.[16, 17] Despite the important discovery of the SET by a hypercoordinate hydridosilicon species, the origin of the reactivity of the process is elusive, due to the paucity of mechanistic studies (e.g., spectroscopic observations and experimental/computational studies). A number of groups[18–21] and Smith et al.[22] recently reported detailed mechanistic studies of a hypercoordinate hydridosilicon species for Lewis-catalysed cross-dehydrogenative C–H silylation of heteroarenes. Two different types of mechanisms were simultaneously proposed which involve a silyl radical addition to a double bond of heteroarenes and a heterolytic

deprotonation of C2–H via a hydride transfer from the common pentacoordinate hydridosilicate intermediate. However, the implication of the dual mechanistic nature involving SET and two-electron transfer processes is currently unclear.

In this work, we provide experimental and computational mechanistic support for the HAT from the potassiated pentacoordinate hydridosilicate to vinylarenes in the context of both hydrosilylation for small molecule synthesis and polymerization for polymer synthesis. The present work involves a redox-neutral process, specifically focusing on revealing how hydrogen atom from pentacoordinate hydridosilicate species is actually transferred to unsaturated moieties via Lewis base-catalysed, complexation-induced HAT (LBCI-HAT), as opposed to a net oxidative process via a silyl radical or hydride transfer (i.e., the dehydrogenative couplings were always involved in the previous studies mentioned above).[18–21] This study counters the currently proposed, two electron transfer mechanism (i.e., hydride) in net redox-neutral, catalytic alkene and alkyne hydrosilylation under the conditions of Lewis base-activation of hydrosilanes.[23–25] This operationally simple and sustainable catalytic process exploits earth abundant, alkali metals base catalysts (as low as 1 mol %, Supplementary Table 3). Notably, they function not only as a HAT initiator, but also a silyl radical stabilizing group, allowing for highly selective cross-radical coupling. Besides the importance of the new mechanistic insights, the LBCI-HAT reaction with vinylarenes presented in this study is capable of accessing both branch-selective olefin hydrosilylation and styrene polymerization in a highly selective manner, depending on the Lewis base catalyst used (Figure 1b). The outcome of these two processes has merit by virtue of silicon functionality in secondary organosilanes and polymers with silane-end functional groups, which allows further elaboration.[2627282930]

Results

Mechanistic discussion.

The mechanism of the LBCI-HAT process, utilizing Lewis base catalyst and hydrosilanes **I** which bear reasonably strong Si–H bonds (ca. 75–90 kcal/mol),[32–34] differs substantially from the well-established HAT-promoted olefin hydrofunctionalization with transition metal catalysts (Figure 1).[4] Specifically, the nucleophilic activation of **I**, with alkali metal Lewis base catalyst through n–σ* interactions, initially produces alkali metal pentacoordinate silicate **II.**[35] Si–H bond strength of **II** (81.9 kcal/mol) is reduced by 15% relative to **I** (96 kcal/mol), determined at the G3B3 level of theory.[36] The activated hydridosilicate **II** delivers a hydrogen atom ($H^{\bullet}$) to the olefin, mediated by a cation-π interaction (**III**),[37] to provide a putative intimate benzylic and silyl radical anion pair cage **IV** (Figure 2, left) [cf., the donor (carbonyl)/acceptor (pentacoordinate silicate) binding through n(O, N)–σ*(Si) complexation permits silicon to expand its valency, leading to hydride (H^-) transfer (**II** to **VIII** to **IX**),[38] Figure 2, right]. The reaction proceeds further to produce the branch-selective hydrosilylation product **VI** via the cross-radical coupling of the benzylic and silyl radicals within **IV**, and regenerate the alkali metal Lewis base for catalytic turn-over. Although Zare and coworkers established a similar K^+-heteroarene π interaction in the context of a C–H silylation,[21] a mode of Lewis base activation of a Si–H bond leading to the HAT to an olefin, without any further energetic activation (e.g., transition metal-mediated photoredox

catalysis), has not been previously reported. Furthermore, the silyl radical transfer mechanism to heteroarenes[20, 21] is improbable in our vinylarene system to explain the observed regioselectivity. The resulting primary radical or anion from the preferential silyl transfer, if any, is not expected to have β-silyl stabilization effect.[39]

In general, the proposed highly selective cross-radical coupling between two reactive radical species appears challenging because of their intrinsic reactivity and minimal effective concentrations. In the present case, the success of such highly selective cross-radical coupling can be attributed to the formation of the intimate ion pair **IV**. Especially, the attenuated reactivity of the transient, unstable silyl radial with incoming Lewis base can form the relatively stable silyl radical anion (in equilibrium between **IV** and **V**), which possesses the capacity for slow-release of the unstable silyl radical for the coupling. Namely, the "protected radicals" masked with alkali metal Lewis base could dictate the reaction with stable yet transient, benzylic radicals by protecting the radical center from potential radical-mediated reactions to yield **VI**.[40] Interestingly, when highly coordinating agents such as 18-crown-6 ether which can sequester alkali metal cations from **IV** are employed, free radical polymerization takes place, leading to polystyrene **VII** (Figure 2). Together, the reaction strategy depicted in Figure 2 can offer advantages for sustainability and operational simplicity, as well as site- and product-selectivity.[8]

Lewis base catalysts and mechanistic investigations.

The benzylic radicals generated from vinylarenes via LBCI-HAT can engage in two competing reaction pathways (Figure 2, left): branch-selective hydrosilylation (to **2**) and HAT-initiated polymerization (to **3**). To establish the reaction parameters of the LBCI-HAT, we first investigated the origin of the activation mode of the Lewis base catalyst and hydrosilane for HAT, dictating high site- and product-selectivity. Unexpectedly, metal cations played a crucial role in promoting and controlling the reaction pathways. While large metals (i.e., K^+, Rb^+, Cs^+, Ba^{2+}, La^{3+}, and Yb^{3+}) promote the reaction, small cations (i.e., Li^+ and Na^+) were unable to catalyse the reaction or did so inefficiently [20] (Figure 3a). Initial screening of Lewis base revealed that not only the widely-used oxyanions (entries 1–4),[18, 19] but also various anionic bases such as amide (entry 5), enolate (entry 6), and hydride (entry 7) were effective for the hydrosilylation. Overall, the LBCI-HAT was generally efficient when the *p*Ka of the corresponding acid of Lewis base is greater than ca. 11 (e.g., β-keto ester potassium enolate, entry 6). Among them, KO^{t}Bu was found to be most effective, which can be lowered down to 1 mol % (70%, 80 °C, 40 h; Supplementary Table 3). When 18-crown-6 (20 mol %) was doped to the reaction mixture (entry 9), complete polymerization was observed to afford polystyrene **3a**. The result indicates that the departure of the cation from the ion pair cage triggers the fragments from **IV** (Figure 2), leading to a free radical polymerization manifold to afford **3a**. In this study, solvent was indeed not necessary for both hydrosilylation and polymerization or if needed, non-polar solvents that have Snyder polarity index < ca. 5 were generally more compatible (Supplementary Table 4).

Addition of several radical initiators to our reaction conditions in the absence of KO^{t}Bu, led to the exclusive styrene polymerization (Supplementary Figure 11), strongly suggesting that

the LBCI-HAT does not generate a transient, free benzylic radical, although it could reside in an ion pair cage (cf., Figure 2, left). To validate the formation of the benzylic radical by HAT, radical trapping agents, TEMPO and galvinoxyl radical were added to the reaction mixture (Figure 3b and 3c, respectively), where TEMPO adduct **5b** and reduced galvinoxyl **6** were isolated. An excess of molecular oxygen also inhibited the reaction. In addition, classical radical clock experiments were carried out. When α-cyclopropyl-substituted styrene **1c** was subjected to the identical conditions, the ring-opened product **7c-Et** was only produced in 81% yield (Figure 3d). When $HMe_2SiOSiMe_2H$ was used, which produces smaller silane HMe_2SiO^tBu *in situ* after reacting with KO^tBu, to our surprise, the non-rearranged benzylic radical was kinetically trapped to afford **2c-Me** along with the rearranged adduct **7c-Me**. The occurrence of the rearrangement adduct is indicative of the presence of the benzylic radical species, produced through a preceding HAT to the β-position of styrene. Furthermore, the non-rearranged adduct allows one to approximate the rate of the silyl radical addition to the benzylic radical after the HAT (cf., cyclopropylbenzyl radical, $k_{ring\text{-}opening} = 3.6\times10^5\ s^{-1}$ at 22 °C). [41] A control experiment with β-cyclopropyl styrene **1d** demonstrated that the HAT occurred at β-position of **2d-**Et and **2d-**Me (Figure 3e). On the other hand, alkyl-substituted alkenes were completely inert toward the LBCI-HAT-mediated hydrosilylation, inferring that the proposed cation-π interaction involving arene next to the olefin is key for the LBCI-HAT. Furthermore, it was not successful to trap the carbon-center benzylic radical via a 6-*exo*-*trig* radical cyclization (Supplementary Figure 21), which implies that the LBCI-HAT does not produce a free benzylic radical, but an intimate radical-radical anion pair cage. In this scenario, the cross-radical coupling within the cage can be feasible by the slow-release of silyl radical from the Lewis base-protected radical anion, as depicted in Figure 2. Next, we turned our attention to the LBCI-HAT-initiated polymerization of styrene. In general, spontaneous polymerization of electron-deficient vinylarenes was observed under the LBCI-HAT conditions; 4-chlorostyrene **1e** provided the polystyrenes **3e** (M_n 27,600; PDI 2.64) in complete conversion (Figure 3f). The more exciting result was that polymerization of electron-rich vinylarenes was in turn achievable by an addition of 18-crown-6, which permitted the polymerization of 4-methoxystrene **1a** to afford **3a** (M_n 10,400; PDI 1.46) with complete conversion (Figure 3g, cf., **IV** to **VII** in Figure 2). To gain a better understanding of the reaction mechanism, we performed the following experiments: (1) To verify the regiospecific hydrogen atom transfer, the reaction between dideuteriodiphenylsilane and **1a** was carried out (Figure 3h). The quantitative transfer of deuterium to the homobenzylic position to afford **2a-**Ph-d_2 was observed. (2) Parallel and competition KIE experiments with **1a** and H_2SiPh_2 and D_2SiPh_2 showed a primary isotope effect of 2.28 and 2.35, respectively, implying that the turn-over limiting step probably involves the cleavage of a Si–H bond (Figure 3i). The present study suggests that LBCI-HAT is feasible only with the larger metal Lewis base catalysts, and a cation-π interaction dictates the reaction pathways (**1** to **2** vs. **1** to **3**).

Cation-π interaction in the LBCI-HAT.

To investigate the interaction of K^+ and π system present in the olefins which is likely essential for the LBCI-HAT, the following experiments were carried out. The reduction of TEMPO radical was utilized as an indicator of HAT (Figure 4A).[42] First, the hydrogen atom trap with TEMPO in the absence of a π donor largely failed, suggesting that the HAT did not

occur (Figure 4a). Secondly, upon addition of styrene as a π donor the HAT was initiated, where the reduced TEMPO was observed (Figure 4b). Finally, to our surprise addition of 18-crown-6 in the absence of a π donor manifested the HAT to furnish more reduced TEMPO (Figure 4c) than the experiment with styrene (Figure 4b). We attribute more facile HAT under the reaction conditions presented in Figure 4c to the stronger interaction of K^+ with the crown ether (cf., vinylarene). These series of experiments suggest that the LBCI-HAT is essentially associated with the cation-π or cation-n interaction.

Spectroscopic studies for the LBCI-HAT.

To directly identify reaction intermediates, experiments exploiting ^{1}H NMR spectroscopy were performed. First, Lewis base [e.g., potassium L-mentholate **8**] reacted with H_2SiEt_2 to quickly produce the (LB)$SiEt_2$H **9** and $(LB)_2SiEt_2$ **10** (ca. 2:1 of **9** and **10**) (Figure 5a). When **1a** was added to the reaction mixture, the reaction immediately turned red and eventually afforded **2a** in 4 h. Second, further insights into the Lewis base (i.e., KH)-catalysed silane disproportionation were gathered by carrying out the reaction of **9** and KH (Figure 5b). The previously observed **10** was formed slowly, along with a formation of H_2SiEt_2. After 16 h, the reaction provided ca. 3:1 of **9** and **10**. A subsequent addition of **1a** to the mixture at 80 °C furnished **2a**. In both experiments, homosilaketal **10** was formed, but it was unclear whether formation of **10** was reversible or not. To establish the reversibility and examine a catalyst consuming route (i.e., **8** to **9** to **10**), **10** was independently prepared and reacted with KH (Supplementary Figure 15). However, **9** was not formed even at elevated temperatures, and an addition of **1a** to the reaction mixture did not effect the hydrosilylation. Together, these observations indicate that Lewis base first reacts with dihydrosilane to quickly produce the 1:1 LB-silane adduct (**9**) and the 2:1 LB-silane adduct (**10**). Only **9** is responsible for the hydrosilylation. Importantly, the addition of vinylarene triggers the LBCI-HAT to furnish **2a**. Lewis base is consumed by the reaction with H_2SiEt_2 to afford **10**, which is not a silane donor for the hydrosilylation and does not return to the catalytic cycle (off-cycle).

EPR spectroscopic experiments were performed in an attempt to directly detect radical intermediates in HAT reactions. However, due to the remarkably short lifetime of the silyl and carbon-centered radicals at ambient temperature, the EPR data collected under the LBCI-HAT conditions exhibited no discernible features either before or after initiation of reaction (Figure 5c). To circumvent the kinetic masking of radical intermediates in the HAT reactions radical, trapping agents[43–46] 2,6-di-*tert*-butyl-4-[(4-hydroxy-2,5-di-*tert*-butylphenyl)-methyl]phenol ($\mathbf{6_{H2}}$) and reduced galvinoxyl radical **6** were added to the reactions. With the former being a spin trap agent, a clean triplet signal centred at an isotropic *g*-value (g_{iso}) of 2.006 was observed within 10 min of reaction initiation. The observed *g*-value, hyperfine splitting pattern, and magnitude of A_{iso} [4.5 MHz] were all consistent with the corresponding radical shown in Figure 5c. When the second radical trap **6** was used in equivalent experiments, a unique radical signal distinct from the known spectra of the $\mathbf{6}^{\bullet}$ was observed (shown in Figure 5d), suggesting a modified radical derivative of **6** was produced instead. Based on the observed spectroscopic properties (e.g., multiline hyperfine splitting and relative intensity of satellite transitions) this signal is tentatively assigned to a potassiated paramagnetic species (^{39}K, I = 3/2) (Supplementary

Figure 18, *Sim 6b*). These EPR experiments demonstrate the accumulation of radical-trapped species.

The above spin-trap experiments are consistent with the radical mechanism in the hydrosilylation involving the LBCI-HAT; however, the most compelling evidence for the proposed mechanism is the direct detection of transient radical species produced in the absence of spin-trapping reagents. Rapid freeze-quench frozen samples were prepared for LBCI-HAT reactions and analyzed by X-band EPR under cryogenic conditions (4–50 K). As shown in Figure 5e (*trace* **10**), two radical species can be observed with average *g*-values (g_{ave}) of 2.006 and 1.993 in samples quenched within 5 seconds. At first glance this spectrum appears much like a doublet split by 2.2 mT (62 MHz). However, the higher field resonance at g_{ave} = 1.993 is absent in samples quenched at 10 and 30 seconds, indicating this species decays more rapidly. These studies are consistent with the aforementioned radical-trap experiments and directly confirm the formation of at least two unique transient radical species in LBCI-HAT reactions in the absence of spin-trapping reagents. At longer time points, the g_{ave} = 2.006 species accumulates, reaching maximum concentration (8.4 μM) 10 minutes after initiation of reaction (Fig. 5e, trace **11**). Spin-quantitation of this signal verifies both its rapid formation, but also that it maintains a near steady-state concentration throughout the time course of the HAT reaction. The observed hyperfine signal intensity (1:2:1) and splitting [A_{iso} = 38 MHz (1.4 mT)] indicate that two equivalent protons are closely associated with the unpaired electron. However, it is unclear if this signal originates from a C- or Si-centred radical.

Computational studies for the LBCI-HAT.

Since the LBCI-HAT mechanism involves the formation of an open-shell free radical pair as the key intermediate, which also competes with a hydride transfer process, we employed multistate density function theory (MSDFT) to characterize the intrinsically multiconfigurational features of reaction pathways.[47–49] The performance of MSDFT on photochemical processes,[47] proton-coupled electron transfer reactions,[49] and singlet-triplet energy splitting of diradicals[48] is comparable to CASPT2 calculations with less computational costs, since dynamic correlation is included first in the configurational states via DFT. On the other hand, although a weighted broken-symmetry approach may be employed with standard Kohn-Sham DFT, it only works well for simple situations and is therefore not well suited to the studied LBCI-HAI reaction.[50] To this end, MSDFT calculations were carried out on the model reactions between Me_2H_2SiR (R = OMe or H) and styrene, CH_2CHPh, with and without K^+ as the alkali metal ion. In MSDFT, a total of seven to eleven determinant configurations for the reactions with or without the metal cation, respectively, were included in the multiconfigurational active space. In the calculation, each configuration represented the spin-adapted singlet and triplet biradical states for the HAT, electron transfer and hydride transfer processes (Supplementary Table 7), and energies of the adiabatic ground and excited states were determined. In essence, Figure 6 depicts a Shaik-like diagram[51–53] that correlates the transition from a closed-shell reactant state of single determinant character to the product with diradical and multiconfigurational character; note that it does not imply that the reaction takes place in the excited state.

The calculations showed that K^+ binds the reactant CH_2CHPh via a cation-π complex that forms a salt-bridge with the pentacoordinate silicon species (Figure 6). The computed reaction barriers are 16.3 kcal/mol for R (i.e., LB) = OMe and 13.9 kcal/mol for R = H (Figure 6a and Supplementary Table 7) using the PBE0 density functional[54] and 6–311++G(d,p) basis set. Interestingly, there was essentially no effect on the barrier height with the inclusion of the K^+ ion, suggesting that there is little charge variation from the reactant to the transition state on the styrene substrate to alter cation-π interactions. However, K^+ provides a remarkable stabilization of the diradical intermediate/product state by more than 50 kcal/mol (Figure 6a), highlighting the importance of cationic counterion in the reaction. We have computed the Coulson structural weights of the electronic states to gain an insight on their relative contributions to the adiabatic potential energy surface (Supplementary Table 7). In all cases, the reactant state complexes were dominated by the closed-shell pentacoordinate silicon anion. The transition state structures were of highly multiconfigurational character, consisting of 60–70% of biradical character mixed with about equal contributions from the closed-shell reactant and product configurations, whereas the hydrogen-transfer intermediates comprised about 75% of the hydride transfer configuration and 25% of biradical character. Importantly, for the reaction with K^+, the energy difference between the singlet ground and triplet excited states was reduced from about 100 kcal/mol in the reactant state to about 40–50 kcal/mol in the hydrogen transfer intermediate (Figure 6a), corresponding to emission of red light, further highlighting the importance of multiconfiguration interaction.

Taken together, all of the experimental and computational studies presented provide new insights into transition metal-free, branch-selective vinylarene hydrosilylation involving the LBCI-HAT. Our observations were consistent with the previous studies, where the alkali metal ion-substrate complexation is key for the atom transfer (hydrogen radical in this study vs. silyl radical[20] or hydride[20,21] by other studies) from pentacoordinate hydridosilicates. In our mechanistic studies, NMR studies identified ionic reaction intermediates in the hydrosilylation and EPR experiments supported the radical mechanism of the LBCI-HAT by observing a potassiated paramagnetic species in radical-trap experiments and the direct detection of transient radical species produced in the absence of spin-trapping reagents. Furthermore, MSDFT revealed a high HAT character, yet multiconfigurational nature in the transition state of the reaction, accounting for the dual mechanistic nature proposed by other researchers.[20, 21]

Scope of the LBCI-HAT, branch-selective hydrosilylation and polymerization of vinylarenes.

Smaller, electron-donating dihydrosilanes generally induced efficient hydrosilylation (**2a-Me** to **2a-MePh**, Figure 7a), while primary or tertiary silanes gave hydrosilylation products in low to moderate yields (Supplementary Table 1). Although LBCI-HAT-initiated polymerization was observed with electron-deficient vinylarenes, the majority of electron-neutral and -rich vinylarenes, including mono and di-substituted styrenes furnished branched products (**2b, 2g-2q**) exclusively (Figure 7b). In cases of *ortho*- or *meta*-substituted styrenes (**1g-1k**) and *ortho*-, *para*-di-substituted substrates (**1r**), TMDSO substantially improved yields. Hindered, 1,2-disubstituted alkenes (**1s-1v**) and trisubstituted alkene **1w** required

elevated temperature. Dual hydrosilylation of acetal-tethered bis-styrene **1x** was achieved to produce **2x** (93% yield). Next, we studied vinyl-substituted heterocycles; a single catalytic protocol exploiting the Lewis base permitted mono-olefin hydrosilylation and dual olefin hydrosilylation and cross-dehydrogenative C–H silylation[18] of 5-vinylindole and 5-vinylbenzofuran. The hydrosilylation occurred first at room temperature to afford **2y** (68% yield) and **2z** (60% yield, ca. 2:1 of **2z**:**2ab**). Upon mild heating cross-dehydrogenative silylation of **2y** and **2z** provided **2aa** and **2ab** (47% and 35% yield, single-pot). Consistent with the LBCI-HAT mechanism proposed, the exceptional chemoselectivity by differentiating aryl- versus alkyl-substituted alkenes was observed within **1ac**. Intramolecular hydrosilylation with KH produced tetrahydrobenzosiline **2ad**, where the reaction with KO^{t}Bu gave a slightly lower yield (65%) due to formation of a minor LB-silane addition adduct, previously observed in our NMR studies (cf., **9**, Figure 5a). We would suggest that KH is better catalyst for intramolecular hydrosilylation via LBCI-HAT, because of the reversible nature of the catalyst. Finally, to validate the viability of the LBCI-HAT-mediated late-stage modification of complex bioactive natural products leading to their biologically relevant analogues, readily accessible styrenes derived from the natural products, steroid (estradiol), vitamin E (δ-tocopherol), terpenoid (geraniol), and amino acid (tyrosine) were subjected to LBCI-HAT conditions to afford hydrosilylation products (**2ae**-**2ah**) with moderate to good yields and exclusive branched regioselectivity.

Conclusions

This work provided the extensive experimental and computational mechanistic studies on the Lewis base-catalysed, complexation-induced HAT (LBCI-HAT) with olefins, harnessing environmentally benign hydrosilane and earth abundant alkali metal Lewis base catalysts. The sustainable LBCI-HAT protocol offers highly selective access to secondary organosilanes or polymers with silane-end functional groups. The mechanistic studies discovered that the cation-π interaction is the key for the LBCI-HAT, specifically how the hydrogen atom and silyl moiety were transferred to unsaturated C–C bonds upon Lewis base catalysis. The dual function of Lewis base catalyst as a HAT initiator and a silyl radical stabilizing group is notable. We anticipate that this study can provide important insights for the finding of more efficient catalytic protocols involving a hypercoordinate silicon species, and can permit to expand the scope of the process for production of new materials and pharmaceutical precursors in a sustainable manner.

Methods

General.

Full experimental procedures for the preparation and purification of all new compounds, complete spectroscopic characterization data for substrates and products and a description of the nuclear magnetic resonance (NMR) (see Supplementary Discussion), electron paramagnetic resonance (EPR) (see Supplementary Figure 17-19) and computational protocols and results (see Supplementary Table 7 and Supplementary Figure 22-23) can be found in the Supplementary Methods.

General procedure for the LBCI-HAT hydrosilylation.

Vinyl arene **1** and hydrosilane were added to a flame-dried vial. Catalyst (i.e., KO^{t}Bu) was added to the mixture (no solvent). The septum on the vial was replaced by a screw cap with a Teflon liner. The solution was kept at the time and temperature indicated in Figure 3 and 6 (external bath). The hydrosilylation product was purified by chromatography on silica gel.

General procedure for the LBCI-HAT styrene polymerization.

Styrene **1**, 18-crown-6, and hydrosilane were dissolved in THF (0.2 M). Catalyst (i.e., KO^{t}Bu) was added to the mixture. Once the polymerization was completed, the polymer was precipitated by addition of methanol to the reaction mixture. After filtration, white solids were washed with cold methanol to provide polystyrenes **3**.

Data availability.

All data supporting the findings of this study, including experimental details, spectroscopic characterization data for all compounds, and computational details, are available within the paper and its Supplementary Information, or from the corresponding author upon reasonable request.

Supplementary Material

Refer to Web version on PubMed Central for supplementary material.

Acknowledgments

We are grateful for financial support from the National Institute of Health (NIGMS, GM116031 to J.J., GM117511–01 to B.S.P.), the ACS Petroleum Research Fund (PRF# 54831-DNI1 to J.J.), and the National Science Foundation (CHE, 1709369 to B.S.P.), Swedish Research Council (VR 2015–04114 to K.N.) and University of Texas at Arlington (to K.N.). The NSF (CHE-0234811 and CHE-0840509) is acknowledged for partial funding of the purchases of the NMR spectrometers used in this work.

References

1. Eisenberg DC & Norton JR Hydrogen-Atom Transfer Reactions of Transition-Metal Hydrides. Israel journal of chemistry. 31, 55–66 (1991).
2. Kumar M, Sinha A & Francisco JS Role of Double Hydrogen Atom Transfer Reactions in Atmospheric Chemistry. Acc. Chem. Res 49, 877–883 (2016). [PubMed: 27074637]
3. Mukaiyama T & Yamada T Recent advances in aerobic oxygenation. Bulletin of the Chemical Society of Japan. 68, 17–35 (1995).
4. Crossley SW, Obradors C, Martinez RM & Shenvi RA Mn-, Fe-, and Co-Catalyzed Radical Hydrofunctionalizations of Olefins. Chemical Reviews. 116, 8912–9000 (2016). [PubMed: 27461578]
5. Mayer JM Hydrogen Atom Abstraction by Metal− Oxo Complexes: Understanding the Analogy with Organic Radical Reactions. Acc. Chem. Res 31, 441–450 (1998).
6. Guallar V, Baik M-H, Lippard SJ & Friesner RA Peripheral heme substituents control the hydrogen-atom abstraction chemistry in cytochromes P450. Proc. Natl. Acad. Sci. U. S. A 100, 6998–7002 (2003). [PubMed: 12771375]
7. Nakajima Y & Shimada S Hydrosilylation reaction of olefins: recent advances and perspectives. RSC Adv. 5, 20603–20616 (2015).
8. Docherty JH, Peng J, Dominey AP & Thomas SP Activation and discovery of earth-abundant metal catalysts using sodium tert-butoxide. Nat. Chem 9, 595–600 (2017). [PubMed: 28537588]

9. Tilset M Crabtree RH, Mingos DMP (ed.) Comprehensive Organometallic Chemistry III Vol. of (Elsevier; 2007).
10. Wiedner ES, et al. Thermodynamic hydricity of transition metal hydrides. Chem. Rev 116, 8655–8692 (2016). [PubMed: 27483171]
11. Lo JC, et al. Functionalized olefin cross-coupling to construct carbon–carbon bonds. Nature. 516, 343–348 (2014). [PubMed: 25519131]
12. Kuo JL, Hartung J, Han A & Norton JR Direct Generation of Oxygen-Stabilized Radicals by H• Transfer from Transition Metal Hydrides. Journal of the American Chemical Society. 137, 1036–1039 (2015). [PubMed: 25569214]
13. Ma X & Herzon SB Intermolecular Hydropyridylation of Unactivated Alkenes. J. Am. Chem. Soc 138, 8718–8721 (2016). [PubMed: 27384921]
14. Green SA, Matos JL, Yagi A & Shenvi RA Branch-Selective Hydroarylation: Iodoarene–Olefin Cross-Coupling. J. Am. Chem. Soc 138, 12779–12782 (2016). [PubMed: 27623023]
15. Colomer E, Corriu RJ & Lheureux M Group 14 metalloles. 2. Ionic species and coordination compounds. Chem. Rev 90, 265–282 (1990).
16. Corriu RJ, Guerin C, Henner B & Wang Q Pentacoordinate hydridosilicates: synthesis and some aspects of their reactivity. Organometallics. 10, 2297–2303 (1991).
17. Shippey MA & Dervan PB Trimethylsilyl anions: direct synthesis of trimethylsilylbenzenes. The Journal of Organic Chemistry. 42, 2654–2655 (1977).
18. Toutov AA, et al. Silylation of CH bonds in aromatic heterocycles by an Earth-abundant metal catalyst. Nature. 518, 80–84 (2015). [PubMed: 25652999]
19. Toutov AA, et al. Alkali Metal-Hydroxide-Catalyzed C (sp)–H Bond silylation. J. Am. Chem. Soc 139, 1668–1674 (2017). [PubMed: 28026952]
20. Liu W-B, et al. KOt-Bu-Catalyzed Dehydrogenative C–H Silylation of Heteroaromatics: A Combined Experimental and Computational Mechanistic Study. J. Am. Chem. Soc 139, 6867–6879 (2017). [PubMed: 28403611]
21. Banerjee S, et al. Ionic and Neutral Mechanisms for C–H Bond Silylation of Aromatic Heterocycles Catalyzed by Potassium tert-Butoxide. J. Am. Chem. Soc 139, 6880–6887 (2017). [PubMed: 28462580]
22. Smith AJ, et al. Electron-Transfer and Hydride-Transfer Pathways in the Stoltz–Grubbs Reducing System (KOtBu/Et3SiH). Angew. Chem. Int. Ed 56, 13747–13751 (2017).
23. Maifeld SV & Lee D Unusual Tandem Alkynylation and trans-Hydrosilylation To Form Oxasilacyclopentenes. Org. Lett 7, 4995–4998 (2005). [PubMed: 16235941]
24. Gatineau D, et al. N-heterocyclic carbene-initiated hydrosilylation of styryl alcohols with dihydrosilanes: a mechanistic investigation. Dalton Trans. 42, 7458–7462 (2013). [PubMed: 23459715]
25. Ilies L, Tsuji H & Nakamura E Synthesis of benzo [b] siloles via KH-promoted cyclization of (2-alkynylphenyl) silanes. Org. Lett 11, 3966–3968 (2009). [PubMed: 19658432]
26. Mandal SK & Roesky HW Group 14 hydrides with low valent elements for activation of small molecules. Acc. Chem. Res 45, 298–307 (2011). [PubMed: 21882810]
27. Brunel JM Polysilanes: The grail for a highly-neglected hydrogen storage source. Int. J. Hydrogen Energy 42, 23004–23009 (2017).
28. Peng W, et al. Silicon surface modification and characterization for emergent photovoltaic applications based on energy transfer. Chem. Rev 115, 12764–12796 (2015). [PubMed: 26244614]
29. Mutahi M. w., Nittoli T, Guo L & Sieburth SM Silicon-Based Metalloprotease Inhibitors: Synthesis and Evaluation of Silanol and Silanediol Peptide Analogues as Inhibitors of Angiotensin-Converting Enzyme1. J. Am. Chem. Soc 124, 7363–7375 (2002). [PubMed: 12071745]
30. Ting R, Adam MJ, Ruth TJ & Perrin DM Arylfluoroborates and Alkylfluorosilicates as Potential PET Imaging Agents: High-Yielding Aqueous Biomolecular F-Labeling. J. Am. Chem. Soc 127, 13094–13095 (2005). [PubMed: 16173707]
31. Simoes JM & Beauchamp J Transition metal-hydrogen and metal-carbon bond strengths: the keys to catalysis. Chem. Rev 90, 629–688 (1990).

32. Kanabus-Kaminska J, Hawari J, Griller D & Chatgilialoglu C Reduction of silicon-hydrogen bond strengths. J. Am. Chem. Soc 109, 5267–5268 (1987).
33. Denmark SE & Beutner GL Lewis base catalysis in organic synthesis. Angew. Chem. Int. Ed 47, 1560–1638 (2008).
34. Couzijn EP, Ehlers AW, Schakel M & Lammertsma K Electronic structure and stability of pentaorganosilicates. J. Am. Chem. Soc 128, 13634–13639 (2006). [PubMed: 17031978]
35. Chuit C, Corriu RJ, Reye C & Young JC Reactivity of penta-and hexacoordinate silicon compounds and their role as reaction intermediates. Chem. Rev 93, 1371–1448 (1993).
36. Baboul AG, Curtiss LA, Redfern PC & Raghavachari K Gaussian-3 theory using density functional geometries and zero-point energies. J. Chem. Phys 110, 7650–7657 (1999).
37. Kumpf RA & Dougherty DA A mechanism for ion selectivity in potassium channels: computational studies of cation-pi interactions. Science. 261, 1708–1710 (1993). [PubMed: 8378771]
38. Boyer J, Corriu R, Perz R & Reye C Reduction selective de composes carbonyles par catalyse heterogene a la surface des sels. Tetrahedron. 37, 2165–2171 (1981).
39. Ibrahim MR & Jorgensen WL Ab initio investigations of the. beta.-silicon effect on alkyl and cyclopropyl carbenium ions and radicals. J. Am. Chem. Soc 111, 819–824 (1989).
40. Fischer H The Persistent Radical Effect: A Principle for Selective Radical Reactions and Living Radical Polymerizations. Chem. Rev 101, 3581–3610 (2001). [PubMed: 11740916]
41. Masnovi J, Samsel EG & Bullock RM Cyclopropylbenzyl radical clocks. J. Chem. Soc., Chem. Commun, 1044–1045 (1989).
42. Mader EA, Larsen AS & Mayer JM Hydrogen Atom Transfer from Iron (II)− Tris [2, 2 ‘-bi (tetrahydropyrimidine)] to TEMPO: A Negative Enthalpy of Activation Predicted by the Marcus Equation. J. Am. Chem. Soc 126, 8066–8067 (2004). [PubMed: 15225018]
43. Dikalov SI & Harrison DG Methods for detection of mitochondrial and cellular reactive oxygen species. Antioxid. Redox Signaling 20, 372–382 (2014).
44. Finkelstein E, Rosen GM & Rauckman EJ Spin trapping. Kinetics of the reaction of superoxide and hydroxyl radicals with nitrones. J. Am. Chem. Soc 102, 4994–4999 (1980).
45. Lalevée J, et al. New photoinitiators based on the silyl radical chemistry: polymerization ability, ESR spin trapping, and laser flash photolysis investigation. Macromolecules. 41, 4180–4186 (2008).
46. Lalevée J, et al. Green bulb light source induced epoxy cationic polymerization under air using tris (2, 2′-bipyridine) ruthenium (II) and silyl radicals. Macromolecules. 43, 10191–10195 (2010).
47. Gao J, Grofe A, Ren H & Bao P Beyond Kohn–Sham Approximation: Hybrid Multistate Wave Function and Density Functional Theory. J. Phys. Chem. Lett 7, 5143–5149 (2016). [PubMed: 27973892]
48. Grofe A, Chen X, Liu W & Gao J Spin-Multiplet Components and Energy Splittings by Multistate Density Functional Theory. J. Phys. Chem. Lett 8, 4838–4845 (2017). [PubMed: 28914545]
49. Cembran A, et al. The Third Dimension of a More O’Ferrall–Jencks Diagram for Hydrogen Atom Transfer in the Isoelectronic Hydrogen Exchange Reactions of (PhX) 2H• with X= O, NH, and CH2. J. Chem. Theory Comput 8, 4347–4358 (2012). [PubMed: 23226989]
50. Luo S, et al. Density functional theory of open-shell systems. the 3d-series transition-metal atoms and their cations. J. Chem. Theory Comput 10, 102–121 (2013).
51. Shaik SS, Schlegel HB & Wolfe S (ed.) Theoretical Aspects of Physical Organic Chemsitry: The SN2 Mechanism. Vol. of (Wiley; New York 1992).
52. Wu W, Su P, Shaik S & Hiberty PC Classical valence bond approach by modern methods. Chem. Rev 111, 7557–7593 (2011). [PubMed: 21848344]
53. Lai W, Li C, Chen H & Shaik S Hydrogen-Abstraction Reactivity Patterns from A to Y: The Valence Bond Way. Angew. Chem. Int. Ed 51, 5556–5578 (2012).
54. Adamo C & Barone V Toward reliable density functional methods without adjustable parameters: The PBE0 model. J. Chem. Phys 110, 6158–6170 (1999).

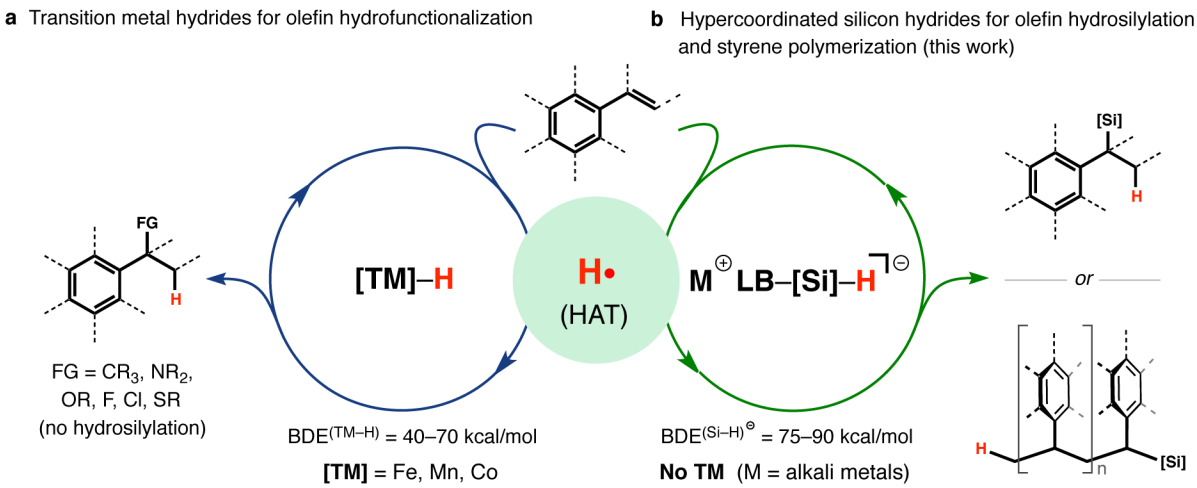

Figure 1 | Strategies to hydrofunctionalization of unsaturated bonds involving transition metal hydride and hypercoordinate silicon hydride catalysis.

a, Advancement in olefin hydrofunctionalization involving HAT as an initiation step to form carbon-centered radicals by transition metal hydrides;[31] BDE, bond dissociation energy; TM, transition metals; FG, functional groups. **b,** Controlled access to branch-selective hydrosilylation of vinylarenes or styrene polymerization involving a sustainable, transition metal-free HAT as an initiation step to form carbon-centered radicals by Lewis base-activated hypercoordinate silicon hydrides;[32–34] LB, Lewis bases.

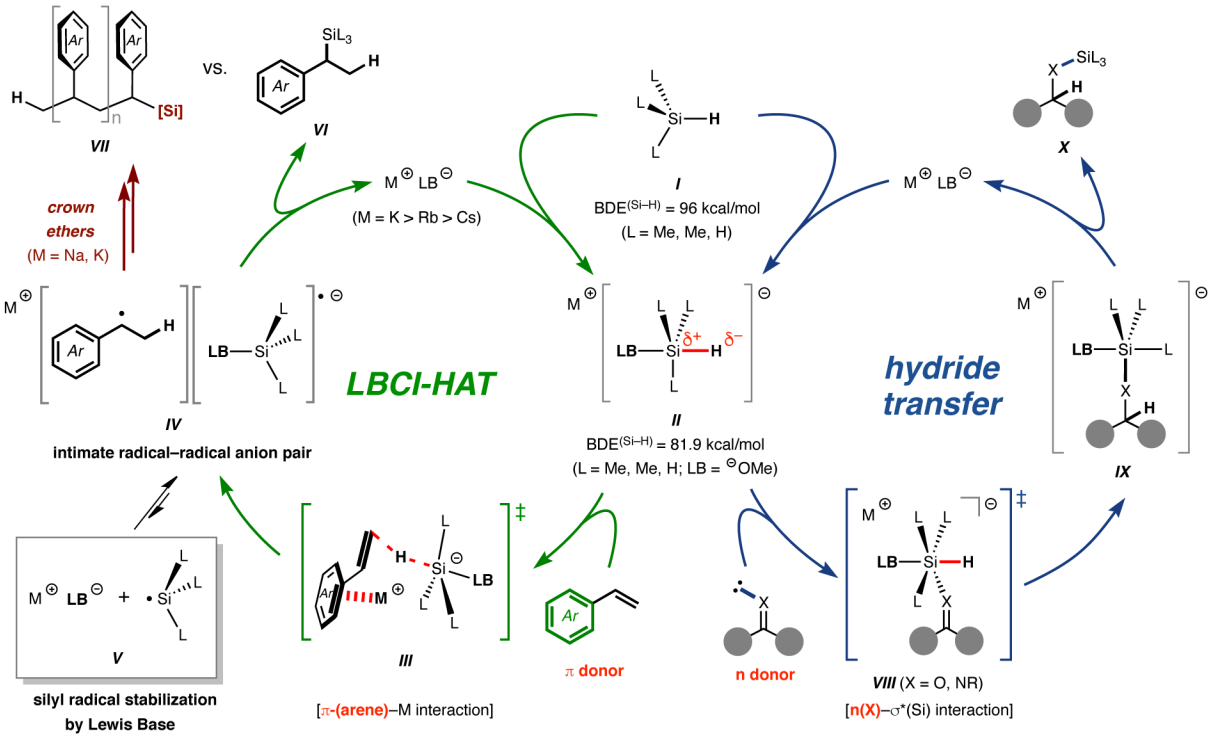

Figure 2 | Proposed mechanism for Lewis base-catalysed, complexation-induced HAT (LBCI-HAT).

Modes of substrate-hypercoordinate silicate interaction, anatomy of a polarized Si–H bond cleavage. Donor (substrate)/acceptor (pentacoordinate silicate) interaction dictates ligand transfer of metal pentacoordinate silicate **II** to give the intimate radical-radical anion pair **IV** (via **III**) or the ligand-exchanged, pentacoordinate silicate **IX** via (hexacoordinate silicate **VIII**) in the Lewis base catalysis; BDE was calculated at the G3B3 level of theory;[36] LB, Lewis bases.

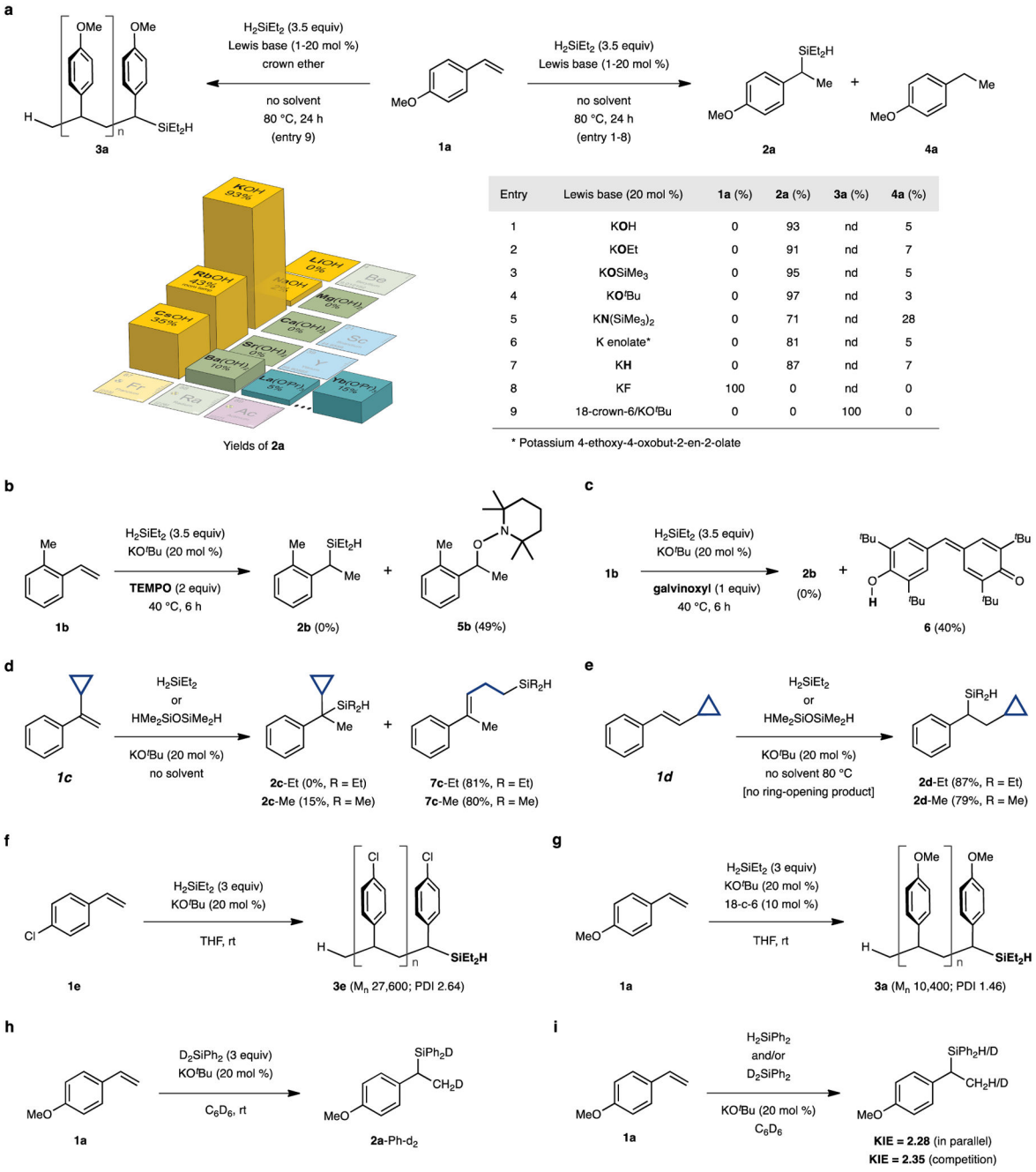

Entry	Lewis base (20 mol %)	1a (%)	2a (%)	3a (%)	4a (%)
1	KOH	0	93	nd	5
2	KOEt	0	91	nd	7
3	$KOSiMe_3$	0	95	nd	5
4	KO^{t}Bu	0	97	nd	3
5	$KN(SiMe_3)_2$	0	71	nd	28
6	K enolate*	0	81	nd	5
7	KH	0	87	nd	7
8	KF	100	0	nd	0
9	18-crown-6/KO^{t}Bu	0	0	100	0

* Potassium 4-ethoxy-4-oxobut-2-en-2-olate

Figure 3 |. Optimization and mechanistic investigation of LBCI-HAT.

a, Survey of Lewis base catalysts and impact of cations using metal hydroxide (MOH) for branch-selective olefin silylation. **b,** Intercepting benzylic radicals generated through the LBCI-HAT by TEMPO. **c,** Capturing hydrogen atom generated through a reaction of Lewis base and diethylsilane by Galvinoxyl. **d,** Radical clock experiments with α-cyclopropyl styrene and diethylsilane/1,1,3,3-tetramethyldisiloxane (TMDSO) indicating that the HAT firstly occurred and then a silyl transfer took place. **e,** Radical clock experiment with β-cyclopropyl styrene. **f,** LBCI-HAT-initiated polymerization of styrene containing an electron-withdrawing group. **g,** LBCI-HAT-initiated polymerization of styrene containing an

electron-donating group assisted by 18-crown-6 ether. **h,** The reaction between dideuteriodiphenylsilane and **1a** gave the quantitative transfer of deuterium to the homobenzylic position to afford **2a**-Ph-d_2. **i,** Primary kinetic isotope effect (KIE) showed that the HAT involving the cleavage of a Si–H bond is the turn-over limiting step.

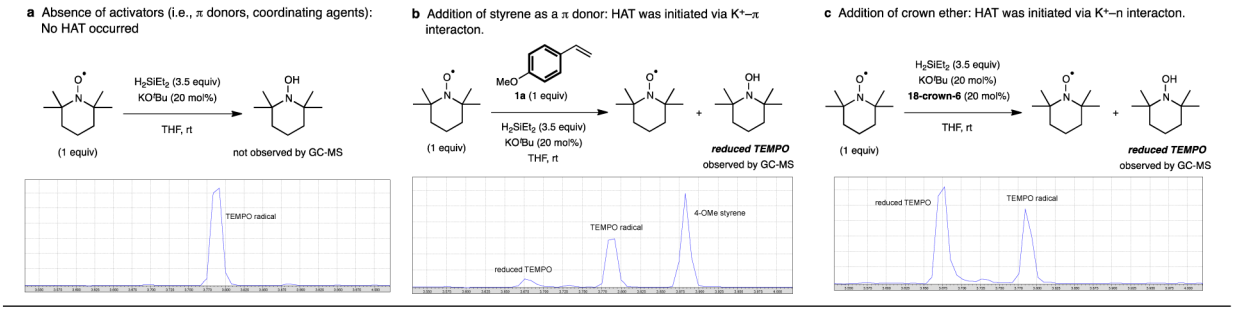

Figure 4 | Hydrogen atom trapping experiments.

Elucidating potassium cation-π interaction in the LBCI-HAT, monitored by GC-MS spectrometry.

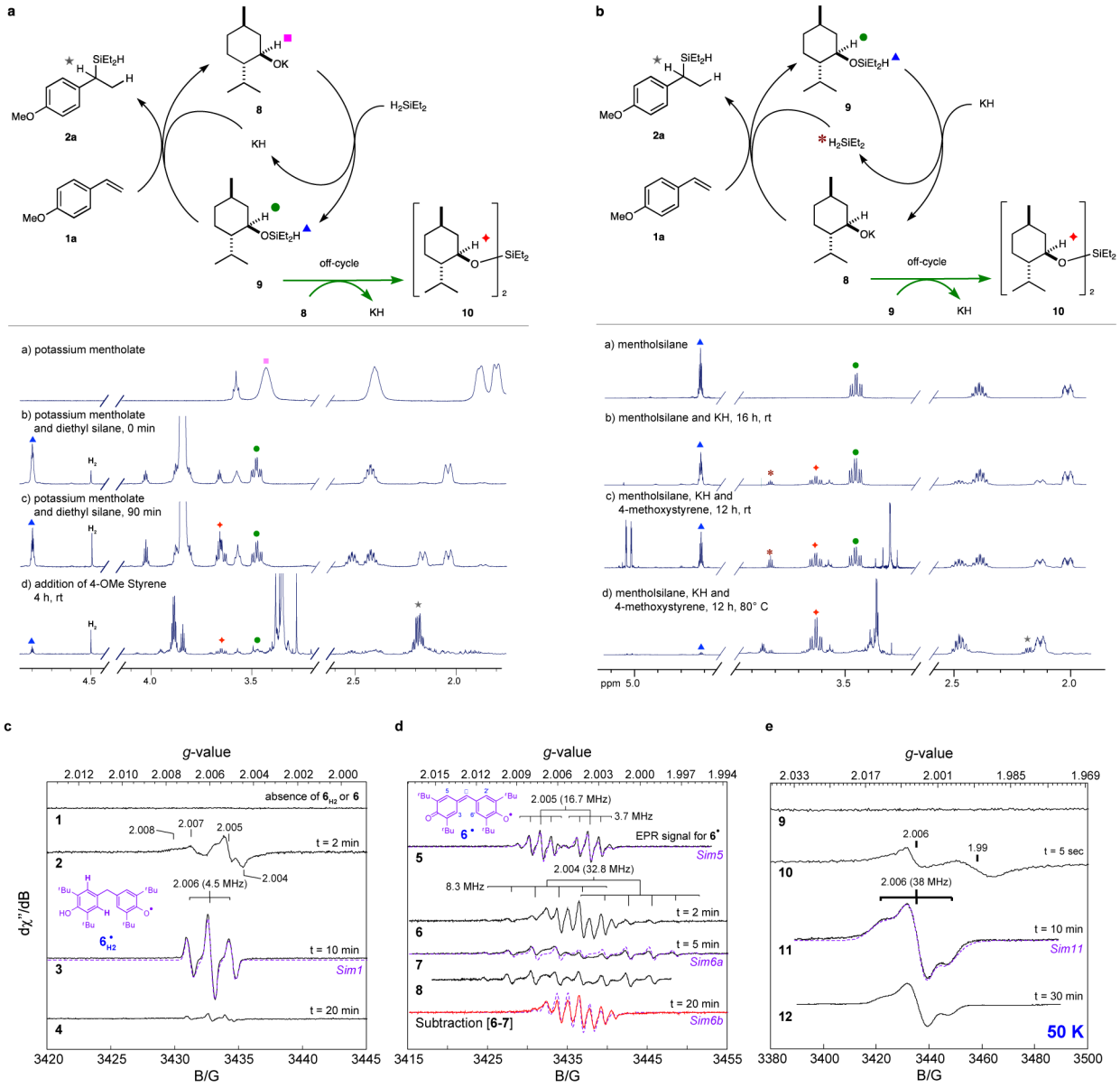

Figure 5 | Spectroscopic studies for the LBCI-HAT.

a, Monitoring the reaction progress with potassium L-mentholate **8** by ^{1}H NMR spectroscopy (500 MHz, C_6D_6) over time. **8** and H_2SiEt_2 were placed in an NMR tube and the reaction was monitored over time. After 90 min, 4-methoxystyrene **1a** was added to the mixture. **b,** Monitoring the reaction progress with potassium hydride (KH, 20 mol %) by ^{1}H NMR spectroscopy (500 MHz, C_6D_6) over time. L-Mentholsilane **9** and KH were placed in an NMR tube and the reaction was monitored over time. After 16 h, **1a** was added to the mixture. H_2 evolution was observed in the beginning phase of the reaction by a reaction of KH and H_2O.[20] **c,** X-band EPR spectra of LBCI-HAT reactions carried out in the presence of $\mathbf{6_{H2}}$ and **6**. Trace 1 illustrates the observed EPR spectra of LBCI-HAT performed in the absence of $\mathbf{6_{H2}}$. Reactions carried out in the presence of $\mathbf{6_{H2}}$ (0.01 mmol) exhibited multiple paramagnetic species which vary with time. Spectra 2, 3, and 4 were collected after 2, 10,

and 20 minutes after initiation of reaction. At 10 minutes a single radical species was observed which ultimately decayed by 20 minutes. **d,** Equivalent reactions carried out using **6** as a spin trap for the LBCI-HAT. Multiple radical species were observed within the first 2 minutes of the reaction (trace 6). Spectra collected at 5 and 10 minutes (trace 7 and 8, respectively) predominately show one radical species with 2-sets of inequivalent ^{1}H-hyperfine coupling patterns. For comparison, the EPR spectrum of the **6**-radical (**6**$^{\bullet}$) is shown in trace 5. **e,** 50 K X-band EPR spectra of freeze-quenched HAT reactions performed in the absence of spin-trapping reagents. Baseline spectra for **1a** in the [diisopropyl ether:isopentane] binary solvent were collected (trace **9**) to confirm the absence of any trace paramagnetic species in the individual reaction components. Equivalent samples were prepared for H_2SiEt_2 and KO^{t}Bu and analysed by cryogenic X-band EPR. For brevity, only the baseline spectra for **1a** is shown as no radical species were observed in any individual reaction component. Traces 10–12 represent freeze-quenched HAT reactions collected at 5-sec, 10-min, and 30-min, respectively.

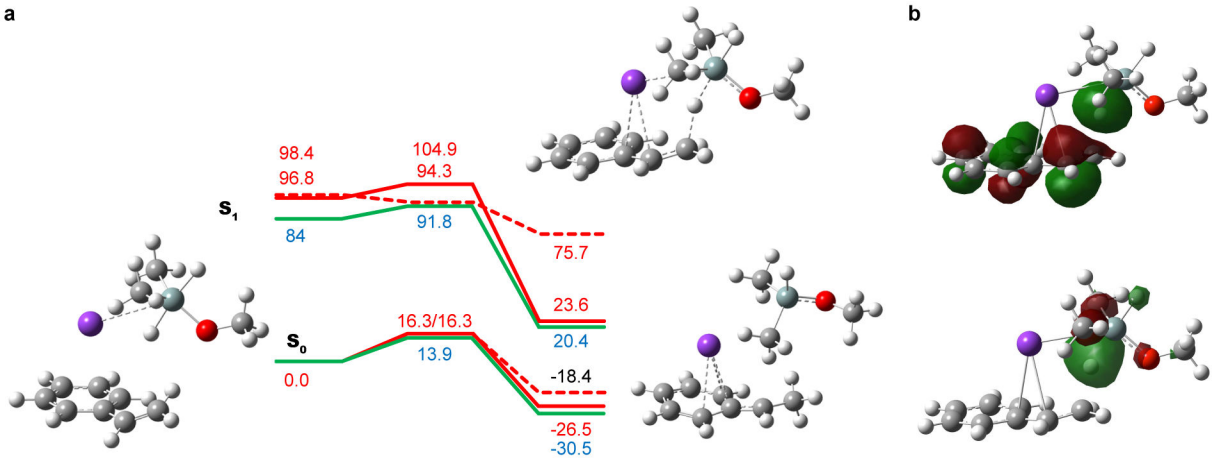

Figure 6 |. Computed reaction energy profile for the LBCI-HAT reactions.

a, Relative energies (kcal/mol) for the reactant state (RS), transition state (TS) and product intermediate (PI) in the singlet ground states (S_0) and excited state (S_1). The reaction of styrene with the pentacoordinate silicon anion Me_2H_2SiOMe is shown in red, and with Me_2H_2SiH is given in green. Solid lines denote the inclusion of a K^+ ion interacting with both reactants and dashed lines for the reaction without K^+. **b,** The two fragment-localized singly occupied molecular orbitals (SOMO) at the transition state where the fragments are defined as $[Me_2HSiOMe]^{\bullet/-}$ ··· $[H\text{-styrene-K}]^{\bullet/+}$, corresponding to a free radical transfer from the silyl anion to styrene-K^+ complex. This is the predominant configuration at the TS with a Coulson structural weight of about 75% for all reactions.

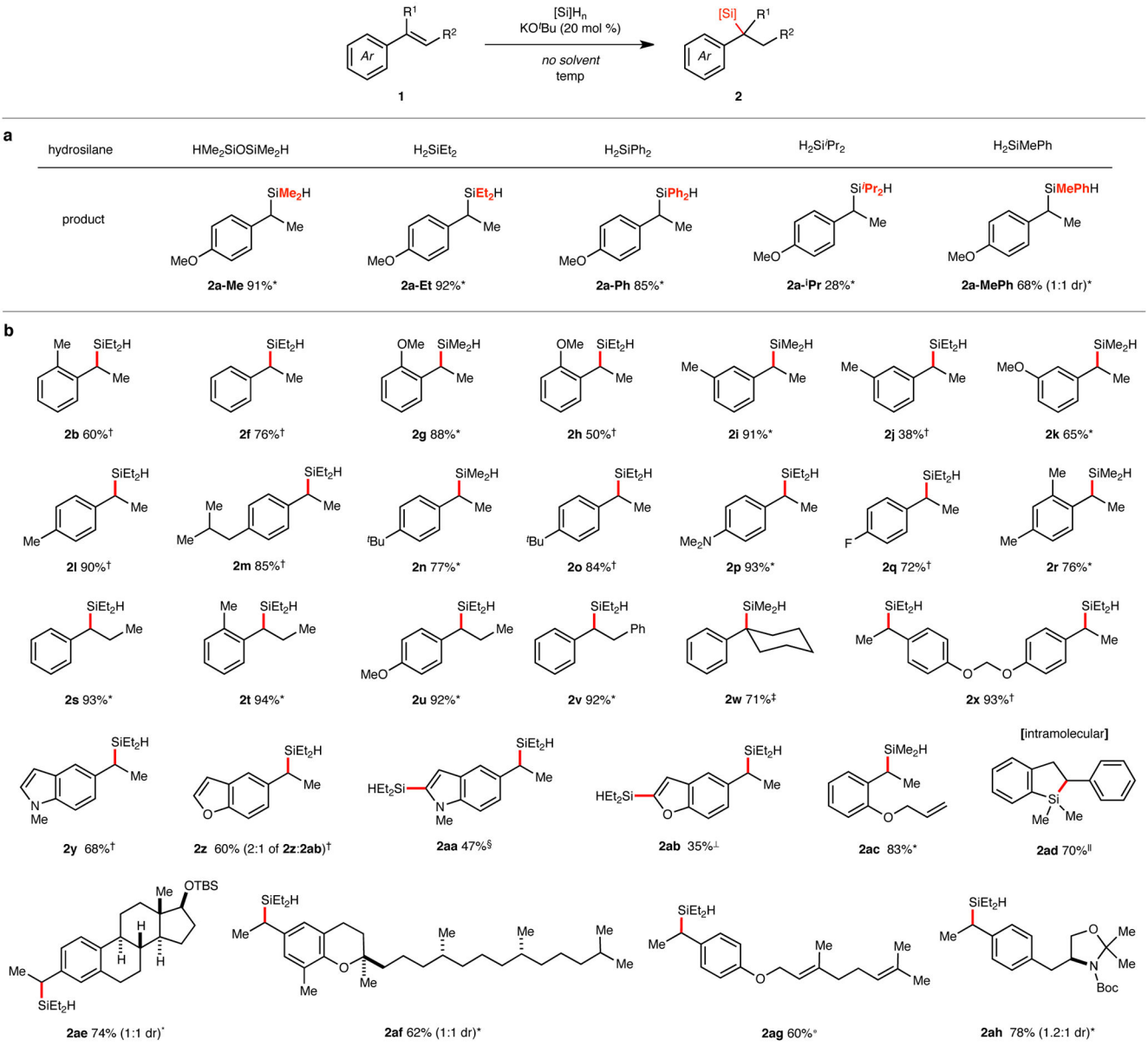

*Conditions: $[Si]H_n$ (3.5 equiv), 80 °C, 12-24 h. Yields are for isolated material. Diastereomeric ratio (*dr*) was determined by ^1H NMR spectroscopy and GC-MS spectrometry analyses of the crude reaction mixture; †Conditions: H_2SiEt_2 (10 equiv), rt, 48 h; ‡Conditions: $O(SiMe_2H)_2$ (5 equiv), 120 °C, 48 h; §Conditions: H_2SiEt_2 (5 equiv), 40 °C, 72 h; ⊥Conditions: H_2SiEt_2 (5 equiv), 80 °C, 48 h; ||Conditions: KH (20 mol %), 80 °C, 12 h.

Figure 7 | Scope of the branch-selective hydrosilylation involving LBCI-HAT.
a, Scope of hydrosilanes **b,** Scope of vinylarenes.